JOURNAL OF THERMOPHYSICS AND HEAT TRANSFER
Vol. 11, No. 4, October–December 1997

Thermocapillary Effects on the Wetting Characteristics of a Heated Curved Meniscus

David M. Pratt*
U.S. Air Force Wright Laboratory, Wright–Patterson Air Force Base, Ohio 45433-7542
and
Kevin P. Hallinan†
University of Dayton, Dayton, Ohio 45409

An investigation of thermocapillary effects on a heated, evaporating meniscus, formed by a wetting liquid in a vertical capillary tube, has been conducted. Experiments were conducted to primarily observe how the wetting characteristics of the working fluid (pentane) are affected by the dynamics associated with the heating of and evaporation from a meniscus. The results have demonstrated that interfacial thermocapillary stresses arising from liquid–vapor interfacial temperature gradients can noticeably degrade the ability of the liquid to wet the pore.

Nomenclature

A_c = internal cross-sectional area of the capillary tube, m^2
c_p = constant pressure specific heat, J/kg-K
g = acceleration because of gravity, m/s^2
h = wicking height, m
h_{fg} = latent heat of vaporization, J/kg
k = thermal conductivity, W/m-K
L = length, m
P = pressure, Pa
Q = heat transfer rate, W
r = radius of the capillary tube, m
T = temperature, °C
V = average liquid velocity, m/s
x = Cartesian coordinate, m
y = Cartesian coordinate, m
γ = slope of surface tension, N/m-K
Δh_{flow} = change in wicking height because of flow losses, m
Δh_{TC} = change in wicking height because of thermocapillary stresses, m
θ = contact angle, deg
μ = absolute viscosity, Pa-s
ρ = density, kg/m^3
σ = surface tension, N/m

Subscripts
b = bottom
conv = convection
l = liquid
lv = liquid–vapor
M = meniscus
r = reservoir
sl = solid–liquid
sv = solid–vapor
TC = thermocapillary
t = top
v = vapor
w = wall
0 = reference

Received Oct. 21, 1996; revision received Feb. 25, 1997; accepted for publication April 4, 1997. This paper is declared a work of the U.S. Government and is not subject to copyright protection in the United States.

*Research Engineer.

†Associate Professor, Department of Mechanical and Aerospace Engineering.

Introduction

HEAT transport devices capable of dissipating high-intensity heat energy as high as 200 W/cm^2 are required for cooling electronics, hypersonic and re-entry vehicles, satellites, propulsion and thermal energy recovery systems, cryoprobes, permafrost stabilizers, roadway de-icers, etc. Of the heat transport devices presently under consideration in this regime, most utilize the latent heat of vaporization via liquid–vapor phase change. Relevant to the present research are passive capillary-driven, phase-change devices.[1] In these devices, the phase change occurs in a liquid saturated porous or grooved media, and capillary forces provide the driving potential for the liquid flow from the condenser to the evaporator. Ultimately, for low-temperature devices, the rate at which the condenser can resupply liquid to the evaporator limits the heat transport. In practice, however, this capillary heat transport limitation is rarely achieved.[2] One possible explanation is that design predictions overpredict the wetting characteristics since they are based on a maximum capillary potential, which presumes that the liquid within the porous structure is perfectly wetting, and static conditions exist at the evaporating menisci. Dynamic effects, other than those caused by viscous flow losses, are not considered.

Objective

The speculation here is that the dynamics associated with fluid motion and heat transport in the vicinity of the evaporating meniscus can detrimentally affect the driving capillary potential by degrading the wetting ability of the working fluid. The change in wettability is speculated to be a result of nonisothermal liquid–vapor interfacial temperatures near the contact line, arising from both nonuniform substrate wall temperatures and nonuniform evaporation. Either or both of these influences yield surface tension gradients on the liquid–vapor interface. These surface tension gradients may result in thermocapillary stresses acting near the contact line, which can degrade the wettability of the liquid.[3–6] Ehrhard and Davis[3] showed that the spreading of a drop on a surface in the direction of increased wall temperature is retarded relative to the spreading of a similar drop on an isothermal surface. Hocking[4] showed that the advancement or spreading of an evaporating drop is retarded because of the evaporation process. Sen and Davis[5] showed that, for a slot configuration, surface tension

gradients create a fluid surface flowfield that also affects the liquid wettability. Anderson and Davis[6] analytically demonstrated that the flowfield was coupled to the temperature field through the thermocapillarity, as discussed by Sen and Davis.[5]

Interestingly, studies of rewetting of liquids along inclined heated plates by Ha and Peterson[7] and Chan and Zhang[8] showed that the maximum wicking height measured was beneath that predicted using the typical Laplace–Young equation by as much as 30%. Given the observations of Ehrhard and Davis,[3] Hocking,[4] Sen and Davis,[5] and Anderson and Davis,[6] it may be that thermocapillary stresses acting near the contact line of the advancing liquid front may inhibit the wetting of the liquid, thereby reducing the wicking height. Thus, the objective of the present work is to determine the effects of thermocapillary stresses on an evaporating liquid–vapor interface within a capillary pore.

Experimental Description

The experiment was designed so that macroscopic wetting characteristics could be observed for a heated and evaporating meniscus within a capillary pore. Specifically, it was designed to determine the effects of thermocapillary stresses near the contact line on the wetting characteristics of evaporating menisci within capillary pores. To accomplish this, a single-pore, capillary-pumped heat transfer device was constructed (Fig. 1). This setup includes a single capillary tube primarily heated from above the meniscus, using an electrical resistance heating element mounted on the o.d. of the tube. The tube is partially immersed in a reservoir of liquid, causing the liquid to partially wick up the tube. The immersion depth of the tube was controlled to provide for consistent positioning of the meniscus. This configuration allowed for use of variable capillary tube diameters. The dimensions for the capillary tubes used during testing are detailed in Table 1. In this table, L is the length of the capillary tube, L_f is the length of the heating element, L_1 is the distance between the bottom of the heater and the first thermocouple, and L_2 is the distance between this thermocouple and another one beneath it. All lengths were measured using a cathetometer, with an associated bias limit of ± 0.0005 cm. The i.d. and o.d. measurements have an error of ± 0.00005 mm and ± 0.05 mm, respectively.

The single-tube, capillary-pumped heat transfer device shown in Fig. 1 was placed within a stainless-steel vacuum chamber with a bell jar lid. The chamber was used to minimize convection losses and possible contamination of the test fluid with air. The chamber was equipped with feed-throughs for thermocouples, heater power connections, and cooling fluid lines. A rotational feed-through was used to control the vertical position of the capillary tube. The entire facility was insulated to provide thermal isolation from the surroundings.

A roughing vacuum pump was used to initially evacuate the system. The liquid reservoir was filled with liquid *n*-pentane, which was chosen because of its relatively low surface energy, high volatility, and excellent wetting characteristics on glass. These qualities are characteristic of the fluids used in capillary-pumped heat transfer devices. To control the temperature of this liquid reservoir, a refrigerated circulator was used to pump cooling fluid through a heat exchanger placed within the reservoir.

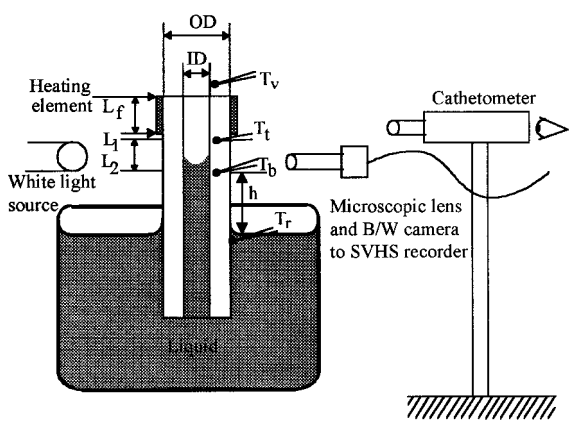

Fig. 1 Schematic of single-pore, capillary-pumped heat transfer device.

A vertical translation system was used to position the meniscus within the capillary tube relative to the heating element, thermocouples, and the end of the vertical capillary tube via a rotational feed-through. As shown in Fig. 1, the immersion depth of the capillary tube was continuously adjusted so that the meniscus base was located at the position of the thermocouple labeled T_b.

The capillary tube was heated using a fine nichrome heater wire (spirally wrapped around the tube at the top) having a resistance of 1 Ω/cm. It was connected to a dc power supply capable of producing up to 3 A at 30 V. A shunt resistor connected in series with the heating element allowed for the current flowing through the heater to be determined by measuring the voltage drop across it.

Calibrated thermocouples were used to measure the wall temperature of the capillary tube, and to measure the temperature of the vapor space and liquid reservoir as shown in Fig. 1. These were recorded using an A/D board interfaced to a 486-66 personal computer. The associated error in the temperature readings were ± 0.3°C with a 95% confidence interval. A video microscope system was used to image the meniscus profile so that the contact angle could be estimated. It consisted of a long-distance microscope connected to a Hi-8 resolution black and white camera. This image was recorded using a super video head system (SVHS) video recorder. The meniscus was backlit with a high-intensity white light source, filtered to allow transmission of light in the green spectrum only, and to block transmission of much of the thermal radiation in the infrared spectrum. This filter was used to optimize the black and white video imaging and to minimize the heating from the light source.

The refrigerated circulator temperature was used to set the liquid reservoir temperature at 10, 19, and 28°C, corresponding to approximately 18, 9, and 0°C of liquid reservoir subcooling, respectively. Tests were run for each of these system states for variable tube diameter and heat input. The test conditions and power inputs for the tests are summarized in Table 2. The data presented in this table include the bulk liquid reservoir temperature and the range of the power input considered.

Table 1 Capillary tube dimensions

i.d., mm		o.d.,	L,	L_f,	L_1,	L_2,
Reference	Actual	mm	cm	cm	cm	cm
0.5	0.4826	6.3	9	1	0.21	0.51
1	0.9906	6.3	9	1.2	0.07	0.65
2	1.77	7.5	9.1	1.2	0.08	0.49

Table 2 Experiment conditions

i.d., mm	Bulk liquid reservoir temperature, °C	Heat input, W
0.5	10.6	0–5.1
0.5	19	0–5.0
0.5	27	0–5.0
1	10	0–5.9, 0–5.0
1	19	0–5.7, 0–5.8
1	28	0–5.4, 0–5.7
2	10	0–5, 0–5.1
2	19	0–3.8, 0–5.1
2	28	0–5.0, 0–5.0

Additional tests were conducted to obtain estimates of the radiation and convection losses from the heated tubes, and to obtain estimates of the impact of heating from below the meniscus and the variations of the wetting characteristics caused by bulk liquid reservoir temperature changes.

Analysis

The most easily measurable macroscopic wetting characteristic of a liquid in a pore is the wicking height. For static interfacial conditions, it can be predicted with the Laplace–Young equation:

$$P_v - P_l = \sigma K \tag{1}$$

The reduced liquid pressure at the meniscus causes the liquid to wick to a height h, which for an axisymmetric pore of radius r, gives rise to the following expression:

$$\rho g h = (2\sigma/r)\cos\theta \tag{2}$$

When the meniscus is heated via wall heating, dynamic effects can alter this wicking height. One effect of heating is to produce a liquid–vapor interfacial temperature gradient near the contact line. This temperature gradient gives rise to a thermocapillary stress, σ_{TC}, emanating from the contact line if the contact line region is hotter than the remainder of the meniscus. Additionally, the evaporative transport from the meniscus because of the heat transfer induces liquid flow from the reservoir. Associated with this flow are viscous losses along the wall of the pore. Both the thermocapillary and the flow loss effects can reduce the wicking height. A vertical force balance is applied to the control volume, defined by the liquid column in the pore shown in Fig. 2 to determine the thermocapillary and flow-loss effects on the capillary potential. This results in the following equilibrium condition:

$$(P_l - P_v)\pi r^2 + (\sigma - \sigma_{TC})2\pi r\cos\theta - \Delta P_{flow}\pi r^2 = 0 \tag{3}$$

with $P_l - P_v = -\rho g h$. Dividing by πr^2, and substituting, yields

$$\rho g h = \frac{2(\sigma - \sigma_{TC})}{r}\cos\theta - \Delta P_{flow} \tag{4}$$

This modified version of the capillary pumping potential incorporates a yet undefined thermocapillary force. The thermocapillary stresses can be estimated from knowledge of the wall-temperature gradient. Previous research has shown that this term has a dominant contribution to the liquid–vapor interfacial temperature gradient for the conditions studied in this experiment. The thermocapillary stress is proportional to the surface tension gradient acting along the liquid–vapor interface, near the contact line over the characteristic length near the contact line, defined as x_0 in Fig. 2. This proportionality is written as follows:

$$\sigma_{TC} \approx \frac{\partial\sigma}{\partial x}x_0 = \frac{\partial\sigma}{\partial T}\frac{\partial T}{\partial x}x_0 \tag{5}$$

Using a linear representation of surface tension with temperature, $\sigma = \sigma_0 - \gamma T$, Eq. (5) can be rewritten as

$$\sigma_{TC} \approx -\gamma\frac{\partial T}{\partial x}x_0 \tag{6}$$

Further assuming that, if x_0 is small such that $\partial T/\partial x \approx \Delta T/x_0 \approx$ const, where ΔT is the interfacial temperature difference over the length x_0, the thermocapillary stress can be finally written as

$$\sigma_{TC} = -\gamma(\Delta T/x_0)x_0 = -\gamma\Delta T \tag{7}$$

The flow pressure drop can be written in terms of the average flow velocity[9]

$$\frac{\Delta P_{flow}}{L_{flow}} = \frac{16}{rRe}\rho\langle V\rangle^2 \tag{8}$$

where $Re = 2r\langle V\rangle\rho/\mu$, and L_{flow} is the flow length from the bottom of the capillary tube to the meniscus. In this equation, the average velocity is related directly to the evaporation rate. This evaporation rate is determinable if the heat transfer into the liquid meniscus, defined as Q_M, can be determined. For the steady-state evaporation process shown in Fig. 3, the heat input to the meniscus region causes both sensible heating and evaporation. A heat balance yields

$$\dot{m}h_{fg} + \dot{m}c_p(T_{sat} - T_r) = Q_M \tag{9}$$

Finally, relating $\dot{m}$ to the average liquid flow velocity up the capillary tube $\langle V\rangle$, and substituting into Eq. (4), yields the following expression for the flow pressure drop:

$$\Delta P_{flow} = \frac{8\mu L_{flow}}{\rho\pi r^4}\frac{Q_M}{h_{fg} + c_p(T_{sat} - T_r)} \tag{10}$$

Combining Eqs. (4) and (10), the expression for the capillary pumping potential for dynamic conditions is

$$\rho g h = \frac{2(\sigma - \sigma_{TC})}{r}\cos\theta - \frac{8\mu L_{flow}}{\rho\pi r^4}\frac{Q_M}{h_{fg} + c_p(T_{sat} - T_r)} \tag{11}$$

Explicitly solving for the wicking height h yields

$$h = h_s - \Delta h_{TC} - \Delta h_{flow} = \frac{2\sigma}{\rho g r}\cos\theta - \frac{2\sigma_{TC}}{\rho g r}\cos\theta - \frac{8\mu L_{flow}}{\rho^2 g\pi r^4}\frac{Q_M}{h_{fg} - c_p(T_{sat} - T_r)} \tag{12}$$

In Eq. (12), h_s is defined as the static wicking height, Δh_{TC} is the reduction in wicking height by thermocapillary stresses at

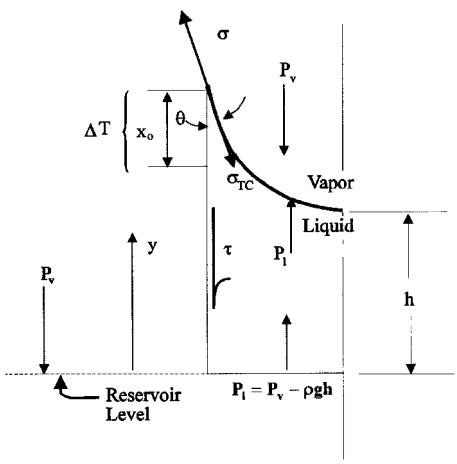

Fig. 2 Meniscus within a capillary tube with an induced temperature gradient.

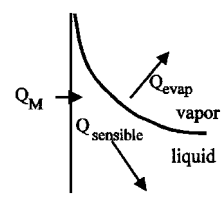

Fig. 3 Heat transfer into the film.

the contact line, and Δh_{flow} is the reduction in wicking height caused by flow losses.

As is apparent from Eq. (12), to determine the effects of thermocapillary stresses on the wicking height, the apparent contact angle θ must be known. The Young–Dupre equation provides a convenient means to determine the contact angle in terms of the surface energies associated with the solid–vapor, the solid–liquid, and the liquid–vapor interfaces, as shown in Eq. (13):

$$\cos\theta = (\sigma_{sv} - \sigma_{sl})/\sigma \tag{13}$$

Of these interfacial energies, σ is the only one affected strongly by temperature changes, decreasing with increasing temperature. Therefore, the measurement of the static contact angle provides a means to estimate the relative difference between σ_{sv} and σ_{sl}.

Data Reduction

In Eq. (6), the near contact line thermocapillary stress was defined in terms of $(\partial T/\partial x)x_0$, where x_0 is some characteristic length along the meniscus in the near contact line. This expression can be related to measurable quantities depicted in Fig. 4, using the following reasoning.

The temperature difference ΔT provides a measure of the wall temperature gradient $\Delta T/L_2$ in the vicinity of the meniscus. Further, assuming that the wall-temperature gradient dominates the interfacial temperature gradient near the contact line,[10] the interfacial temperature gradient near the contact line is then approximately $\Delta T/L_2$. This assumes a roughly constant wall temperature gradient along the capillary tube, so that in Eq. (7), the liquid–vapor interfacial temperature gradient acting over a distance x_0 is written as $\partial T/\partial x \approx \Delta T/x_0 \approx \Delta T/L_2$. However, the liquid–vapor interfacial temperature gradient occurs only over the length x_0, which cannot be bigger than r. Thus, the thermocapillary stress obtained from the experimentally measured data is

$$\sigma_{TC} = -\gamma \frac{\Delta T}{L_2} x_0 \approx -\gamma \frac{\Delta T}{L_2} r \tag{14}$$

Note that substitution of this experimentally measured value for σ_{TC} into Eq. (12) provides a means for obtaining a theoretical prediction of the dynamic wicking height, which includes thermocapillary stresses based on experimentally measured quantities.

Contact Angle

The experimental contact angle was determined from the video images of the meniscus recorded during testing. This image was digitized and enhanced using image processing software. The meniscus was then cropped and magnified to remove aspects of the image not required for determination of the contact angle. A Sobel gradient-edge detection algorithm was then applied to determine the edge locations of the liquid–vapor interface. Compensation for refraction of light by the curved glass capillary tube wall and the test chambers optical window was made. Finally, from the measured coordinate positions, the meniscus curvature was determined. Knowing the curvature and pore i.d., the contact angle could be estimated presuming a spherical meniscus as $K_{meas} = (2/r)\cos\theta$.

Meniscus Heat Input

The heat transfer into the meniscus required that the heat loss to the surroundings be determined. Experiments, described elsewhere,[11] were conducted to determine these losses. Once this was accomplished, the heat transfer into the meniscus was calculated from the measured difference in the axial wall-temperature gradients above and below the meniscus:

$$Q_M = k_g A_c \left(\frac{T_t - T_b}{L_2} - \frac{T_b - T_r}{h} \right) - Q_{conv} \tag{15}$$

Here, k_g is the thermal conductivity of the capillary tube wall material, A_c is the cross-sectional area of the capillary tube, and Q_{conv} is the estimated external convection loss.

Results

The contact angle was determined using the Young–Dupre equation [Eq. (13)]. In using the Young–Dupre equation to predict the static wicking height, the measured contact angle is used to determine the difference between σ_{sv} and σ_{sl}. These interfacial energies are presumed to remain constant as the interfacial temperature increases, whereas the liquid–vapor interfacial energy σ decreases with increasing temperature. The contact angle based upon the measured wicking height, and Eq. (2) where properties were based upon actual experimental conditions, was also determined. Finally, the meniscus images were analyzed to yield an experimental determination of the contact angle. One experimental data set for these is shown in Fig. 5, to illustrate trends associated with the predicted and measured contact angles as a function of meniscus temperature. In Fig. 5, the measured value of the contact angle from the image can only be used to represent the trends in the contact angle, since its accuracy is only ±3 deg. Within this uncertainty, the measured contact angle measured compares very favorably with that predicted using the Young–Dupre equation. Similar measurements supported its use for all test conditions considered; thus, the subsequent results predicting the wicking height are based upon the contact angle predicted using the Young–Dupre equation.

The wicking height was then predicted using Eq. (12) and experimentally measured conditions to estimate the thermocapillary stress and the flow pressure drop. The static wicking height [Eq. (2)] and the dynamic wicking height [Eq. (12)] are

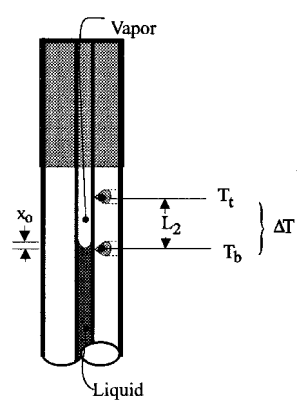

Fig. 4 Capillary tube experimentally determined temperatures.

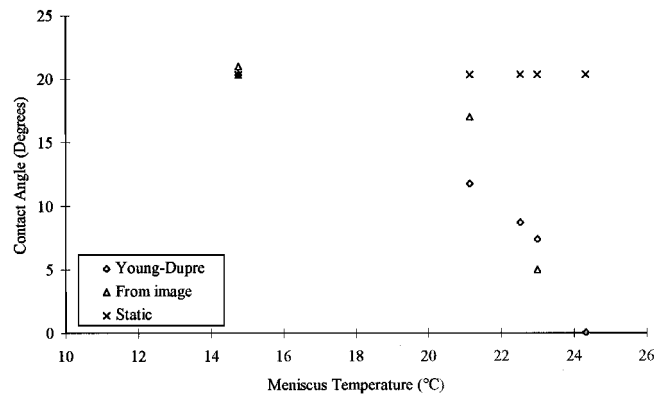

Fig. 5 Contact angle vs meniscus temperature.

compared to the experimentally measured values in the following figures. In these figures, the wicking heights shown have associated errors of ±1% for the measured value, ±0.4% for that predicted by Eq. (12), and ±0.1% for that predicted by Eq. (2), all within a 95% confidence level.

The data presented in Fig. 6 shows the respective wicking heights for the 0.5-mm i.d. capillary pore for a reservoir temperature of 10, 19, and 28°C. This data clearly shows that the static predictions overpredict the experimental measurements. The data additionally show a strong correlation to dynamic wicking height prediction given by Eq. (12), until the wall temperature gradients exceed 100 K/cm. At wall temperature gradients greater than this value, the reduction in wicking height from that predicted using Eq. (12) is substantial. At a wall temperature gradient of 150 K/cm, the measured wicking height is reduced by as much as 50%. It should be noted that above a wall-temperature gradient of 100 K/cm, the meniscus was observed to become unstable, thereafter experiencing significant oscillations. In these cases, the wicking height measured corresponds to the maximum wicking height attained. A discussion of this trend will be provided after presentation of the remainder of the data for the larger pore sizes.

The wicking height data for the 1-mm capillary pore are presented in Figs. 7a–7c, for reservoir temperatures of 10, 19, and 28°C, respectively. These plots represent the wicking heights as a function of the wall-temperature gradient. They again show that the static prediction is unsatisfactory in predicting the measured value, and the dynamic prediction given

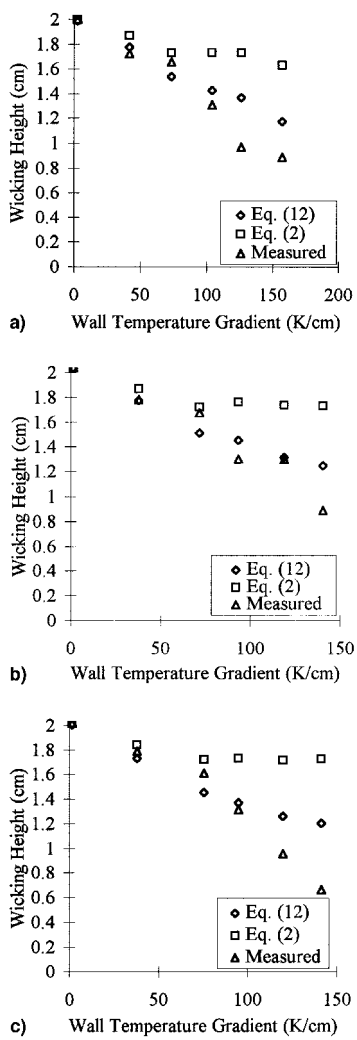

Fig. 6 Wicking height for a 0.5-mm capillary pore at reservoir temperatures of a) 10, b) 19, and c) 28°C.

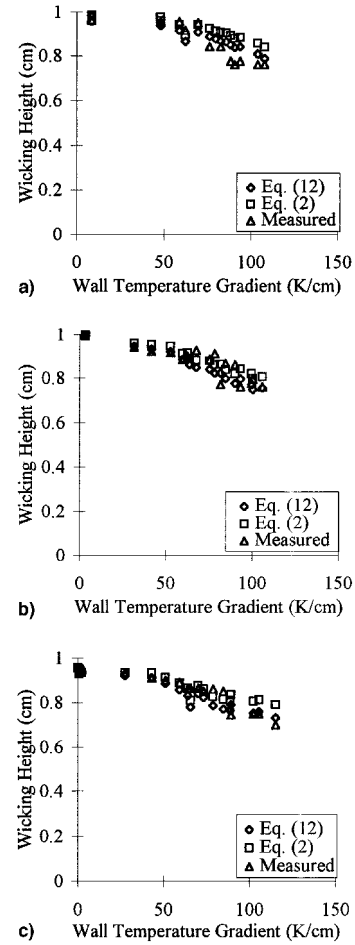

Fig. 7 Wicking height for a 1-mm capillary pore at reservoir temperatures of a) 10, b) 19, and c) 28°C.

by Eq. (12) correlates well with the experimental data, particularly with increasing heat inputs.

The trends realized for the previous pore sizes are additionally supported by similar data for the 2-mm capillary pore. Plots of wicking height vs the wall-temperature gradient for this size are presented in Fig. 8.

The wicking height data presented in the previous figures clearly show that the dynamic prediction of the wicking height obtained from Eq. (12) correlates fairly well with the experimental data, except for the high wall-temperature gradient data for the 0.5-mm pore. Thus, the system dynamics have been shown to noticeably affect the liquids wettability, although the contribution of interfacial thermocapillary stresses to the changes is not apparent from Figs. 6–8.

In Fig. 9, it is apparent that thermocapillary stresses near the contact line are in part responsible for these trends. Figure 9 presents the ratio of changes in wicking height because of thermocapillary stresses [as predicted using Eq. (12)], to the wicking height determined, neglecting their influences for 0.5-, 1-, and 2-mm capillary pores. Figure 9 illustrates that the predicted wicking height reduction as a result of thermocapillary stresses is most significant for the larger pore sizes; a reduction in the capillary pumping potential from that typically considered as high as 12% at wall temperature gradients of up to 150 K/cm for the 2-mm i.d. pore. Even for the smallest capillary pore considered (0.5 mm), where the flow pressure losses are large at comparable wall-temperature gradients, the interfacial thermocapillary stresses result in up to a predicted 5% reduction of the capillary pumping potential from that typically estimated.

To support the conclusion that near contact line thermocapillary stresses can degrade the wettability of a liquid in a heated

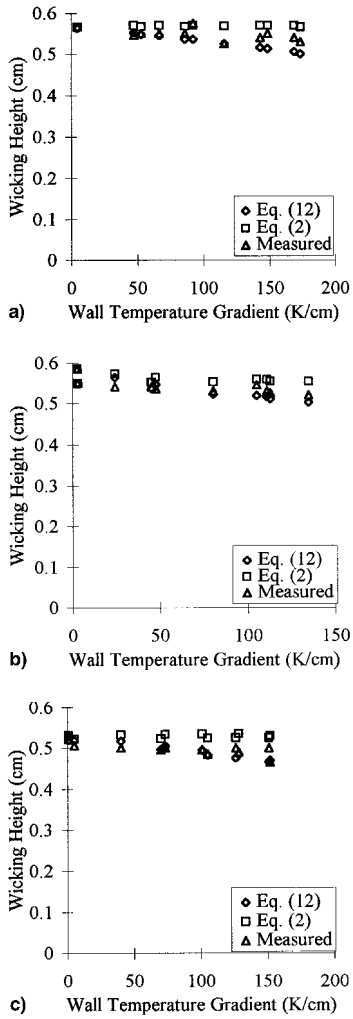

Fig. 8 Wicking height for a 2-mm capillary pore at reservoir temperatures of a) 10, b) 19, and c) 28°C.

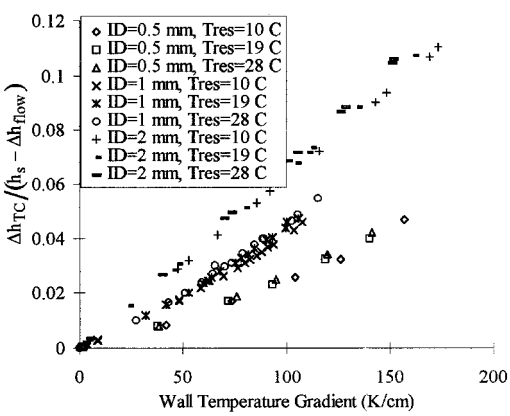

Fig. 9 Reduction in wicking height because of thermocapillary stresses compared to the predicted wicking height ignoring these effects.

pore, tests were conducted with heating from below the meniscus. These experiments produced a wall-temperature gradient in the direction opposite of the initial experiments, and a thermocapillary stress near the contact line acting in a direction toward the contact line. The wicking height data for these tests are shown in Fig. 10, as a function of the wall-temperature gradient for a 1-mm capillary pore at a liquid reservoir temperature of 19 and 28°C, respectively. These figures also include the static wicking height prediction [Eq. (2)], and the dynamic predictions using Eq. (12).

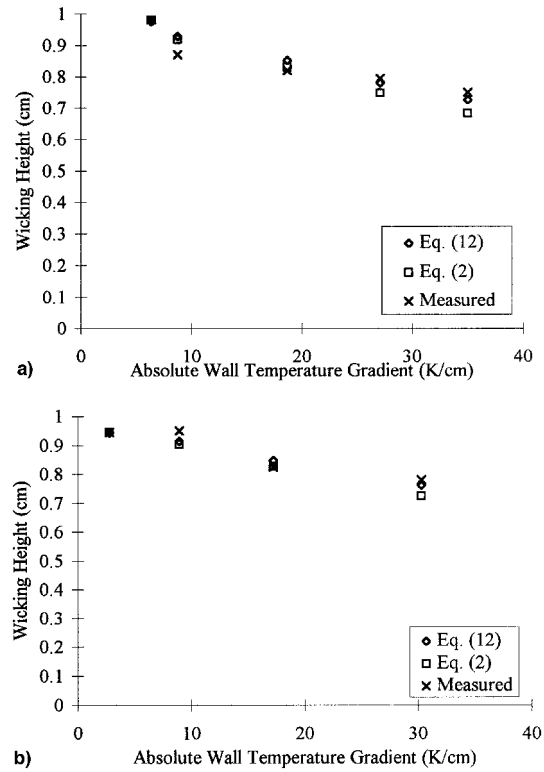

Fig. 10 Wicking height heating from below for a 1-mm capillary pore at reservoir temperatures of a) 19 and b) 28°C.

It is obvious from these figures that the thermocapillary stresses cause the predicted wicking height to be greater than that predicted for static conditions when the heat input is from below the meniscus. The data support these trends.

Conclusions

This work shows that dynamic effects caused by thermocapillary stresses could degrade the wettability of a meniscus if wall-temperature gradients near the contact line of the meniscus are large. For 1- and 2-mm pore sizes, a reduction in the capillary pumping potential because of thermocapillary stresses of up to 12% was observed when wall-temperature gradients exceeded 100 K/cm. For smaller pore sizes, the dynamic influences on the reduction in wicking height were most substantial (up to 50% of that predicted) for very large wall temperature gradients. The pressure-drop calculation given by Eq. (8) may underestimate the actual pressure drop because of the competing influences of the thermocapillary flows near the contact line, inducing flow toward the meniscus centerline, and the evaporation-driven bulk flow seeking to stagnate near the centerline. An alternate explanation may be attributed to the oscillatory meniscus behavior observed at the higher wall-temperature gradients. It may be that during the oscillations, in the period when the meniscus is advancing, the miniscus becomes unstable prior to completely returning, providing the trigger for superheated liquid to evaporate spontaneously. Vapor recoil stresses that are generated may then force a depression of the meniscus. Both ideas merit additional study. It is sufficient at this time, we believe, to report the results that show that the current theory may inadequately describe the capillary potential that exists in real capillary-pumped heat transfer devices.

The reduction in the capillary pumping potential because of the dynamic effects observed, may explain the inability to achieve the predicted maximum heat transfer capability of capillary pumped heat transfer devices. Specifically, the prediction of the capillary pumping potential without regard to these stresses used in design predictions may lead to an overprediction of the heat transport capacity of these devices.

References

[1]Chang, W. S., and Hager, B. G., "Advance Two-Phase Thermal Management in Space," National Heat Transfer Conf., Minneapolis, MN, 1990.

[2]Richter, R., and Gottschlich, J. M., "Thermodynamic Aspects of Heat Pipe Operation," *Journal of Thermophysics and Heat Transfer*, Vol. 8, No. 2, 1994, pp. 334–340.

[3]Ehrhard, P., and Davis, S. H., "Non-Isothermal Spreading of Liquid Drops on Horizontal Plates," *Journal of Fluid Mechanics*, Vol. 229, Aug. 1991, pp. 365–388.

[4]Hocking, L. M., "On Contact Angles in Evaporating Liquids," *Physics of Fluids*, Vol. 7, No. 12, 1995, pp. 2950–2955.

[5]Sen, A. K., and Davis, S. H., "Steady Thermocapillary Flows in Two-Dimensional Slots," *Journal of Fluid Mechanics*, Vol. 121, Aug. 1982, pp. 163–186.

[6]Anderson, D. M., and Davis, S. H., "Local Fluid and Heat Flow Near Contact Lines," *Journal of Fluid Mechanics*, Vol. 268, June 1994, pp. 231–265.

[7]Ha, J. M., and Peterson, G. P., "Analytical Prediction of the Axial Dryout Point for Evaporating Liquids in Triangular Microgrooves," *Journal of Heat Transfer*, Vol. 116, No. 2, 1994, pp. 498–503.

[8]Chan, S. H., and Zhang, W., "Rewetting Theory and the Dryout Heat Flux of Smooth and Grooved Plates with a Uniform Heating," *Journal of Heat Transfer*, Vol. 116, No. 1, 1994, pp. 173–179.

[9]Bird, R. B., Stewart, W. E., and Lightfoot, E. N., *Transport Phenomena*, Wiley, New York, 1960.

[10]He, Q., "A Novel Microscale Flow Field Measurement Technique for Extracting Fundamental Physics of Dynamic Thin Liquid Films," Ph.D. Dissertation, Dept. of Mechanical and Aerospace Engineering, Univ. of Dayton, Dayton, OH, 1996.

[11]Pratt, D. M., "The Effects of Thermocapillary Stresses on the Wetting Characteristics, Heat Transfer Effectiveness, and Stability of an Evaporating, Capillary Re-Supplied, Curved Meniscus Within a Capillary Tube," Ph.D. Dissertation, Dept. of Mechanical and Aerospace Engineering, Univ. of Dayton, Dayton, OH, 1996.